

# COMPARATIVE STUDY OF INDIRECT CURRENT CONTROL METHODS FOR THREE PHASE THREE LEG FOUR WIRE SAPF

<sup>1</sup>: Faculty for Electrical Engineering, University of Craiova, ROMANIA

**Abstract:** The aim of this paper was the implementation and the comparative performance analysis of two variants of the indirect current control algorithm for a three phase four wire active power filter. The implemented variants of the indirect current control obtained the amplitude of the desired power grid current at the output of the voltage controller, and by computing the load current active component amplitude. The two algorithms implementation was firstly validated by simulation, and finally on an experimental active filtering system mounted at the power electronics department of an industrial facility. The experimental active filter control section is based on a dSPACE DS1103 prototyping board, therefore the control algorithm/program of the experimental filter is the same Simulink block as in the virtual active filter. The results obtained on the virtual system proved not only the good performance of the implemented control algorithms, but also similar results. However, the results obtained on the experimental setup show that the control system is highly dependent on the computation time step (the closed loop control system especially) and one variant of the indirect current control is giving better results as it reduces the significance of the voltage controller output in the grid current amplitude.

**Keywords:** indirect current control, prototyping board, power quality, active power filter

## 1. INTRODUCTION

The traditional active power filter topology is the three-phase, three-wire, shunt topology which has the advantage of a lower necessary compensating capacitor voltage, and a simpler control, compared to the four-wire four-leg topology. At the same time it has the disadvantage of the limited capability to compensate heavy unbalanced loads (one current being dependent by the other two) [1–4].

Because the polluting loads which require current compensation are usually are not constant over time, the optimum compensating capacitor voltage is also not constant over time. It thus becomes advantageous the real time adjustment of the compensating capacitor voltage, as a function of the non-active power to be compensated, in order to reduce the transistors switching losses, and to ensure good compensation at the same time [5–6].

Considering the indirect current control, the desired current to be absorbed from the power grid is conditioned by the active power filter. That is, the compensated current shape is defined by the voltage template (i.e. the sinusoidal synchronizing signal with unitary amplitude in phase with the power grid voltage, obtained by means of a phase locked loop). The compensated current amplitude can be obtained in two ways:

- ≡ By the compensating capacitor voltage controller – the voltage controller output signal is the compensated current amplitude (it includes the polluting loads active current component and the active power filter active current necessary to load the compensating capacitor above the power grid voltage amplitude and to cover the power inverter losses) [5–6];
- ≡ The compensated current amplitude is the sum of two components:
  - The active component of the polluting loads current, computed from the polluting loads absorbed active power and grid voltage;
  - The compensated capacitor voltage controller output, which in this case represents only the amplitude of the active current necessary to charge the capacitor and to cover the inverter losses.

For the both approaches, the optimal voltage control consists of real time computation of the compensating capacitor imposed voltage on one hand, and of the voltage controller parameters (proportionality constant, ant integration time constant) on the other hand, as a function of the non-active power to be compensated [5–6].

The two variants of the active power filter control algorithm were implemented and tested by simulation, on an active filtering system virtual model, and further implemented and tested on an experimental environment, using the dSPACE DS1103 prototyping board. It must be mentioned that the experimental nonlinear load consists of the power electronics department of a company from Craiova and it includes a whole range of equipment, active, reactive and nonlinear (such as electric motors, heating resistors, fluorescent lighting tubes, air conditioners, etc.). Therefore for the case of the experimental validation of the control algorithm implementation, the load could not be controlled during the experiments, than to a small extent, as it was dependent on the activity of the industrial facility at the experiment time. To keep the relevance between the

simulation study and the experimental study, the virtual polluting load was built to replicate the experimental load recorded at a random time.

## 2. THE INDIRECT CURRENT CONTROL ALGORITHM

The first variant of the active power filter control algorithm is the indirect current control based on the voltage controller output [5–7]. It contains two cascaded control loops, the desired grid current being obtained by the voltage controller (the amplitude) and the phase locked loop (phase and waveform) – Figure 1–a [5–7]:

- ≡ The compensating capacitor control loop, which gives the power grid desired current amplitude;
- ≡ The power grid current control loop, which obtains the current absorbed from the power grid by the active filtering system.

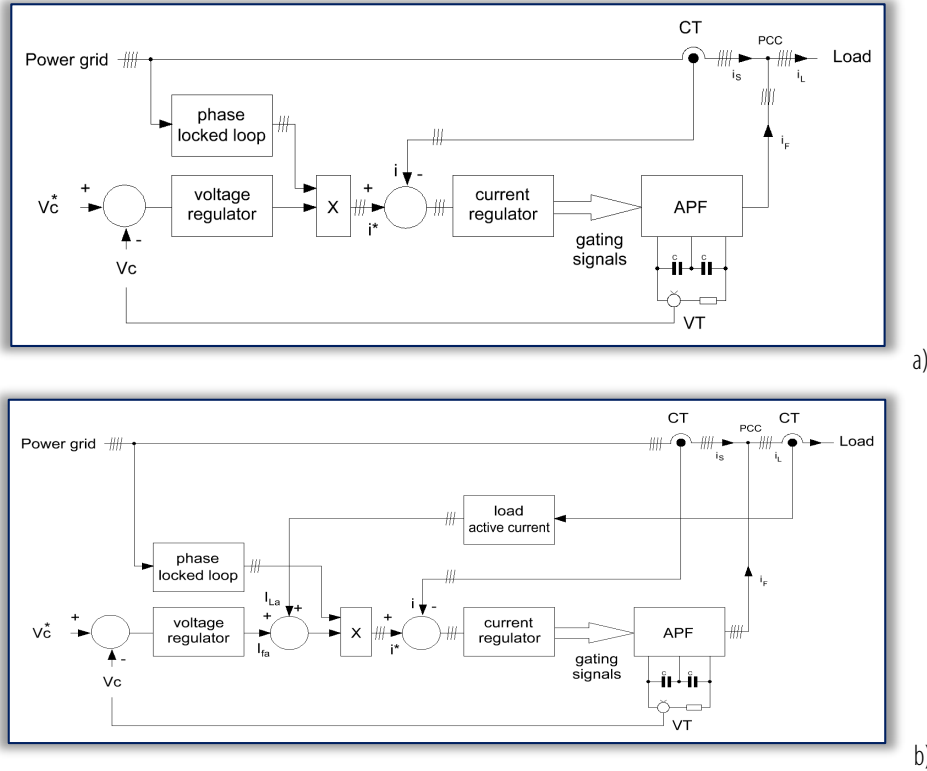


Figure 1. Four wire active power filter control algorithm: a) indirect current control, b) indirect current control with load active current computation

The notations in Figure 1 are:

- ≡  $V_c$  – compensating capacitor voltage (the voltage transducer measured the voltage across both capacitors, connected in series; the central socket is connected to the power grid neutral point);
- ≡ APF – active power filter power section;
- ≡ VT – voltage transducer;
- ≡ CT – current transducer;
- ≡  $i^*$  – power grid desired/imposed instantaneous current;
- ≡  $i$  – power grid instantaneous current.

To reduce the negative effect of the voltage controller output ripple on the compensated current shape (given the high value of this signal), the power grid desired current amplitude is computed as the sum of the voltage controller output ( $I_{fa}$  in Figure 1–b) and the load active current amplitude ( $I_{La}$  in Figure 1–b). The load active current is obtained based on the load active power [6]:

$$I_{LaRMS} = \frac{\sum_{k=1}^3 \frac{1}{T} \int_0^T u_{sk} \cdot i_{Lk} dt}{\sum_{k=1}^3 U_{sk}} \quad (1)$$

where:

- ≡  $I_L$  – load current active component, RMS value;
- ≡  $U_{sk}$  – power grid voltage RMS value of phase  $k$ ;
- ≡  $u_{sk}$  – power grid instantaneous voltage on phase  $k$ ;
- ≡  $i_{Lk}$  – load instantaneous current on phase  $k$ .

For the both current control methods, the voltage controller (proportional–integrative) is tuned based on the modulus criterion [7].

Considering the adaptive capacitor voltage control, the voltage controller parameters are real–time adapted to the non–active power to be compensated [5–7].

The power grid current control loop uses hysteresis type controllers which gives the gating signals for the active filter power transistors. The switching frequency is limited by the hysteresis band on one hand and by the time sample (simulation step) on the other hand.

### 3. CONTROL ALGORITHM VIRTUAL IMPLEMENTATION

The two variants of the control algorithm were implemented in the Matlab Simulink environment, for a complete virtual active filtering system, done to replicate the experimental environment. The power section (identical for the two variants of the control algorithms) of the active filtering system was built with SimPowerSystems blocks. The specific sections of the schematic had been grouped in masked subsystems. The control section was also grouped in a Simulink subsystem, for easy migration from one algorithm variant to the other. The complete active filtering virtual system is illustrated in Figure 2.

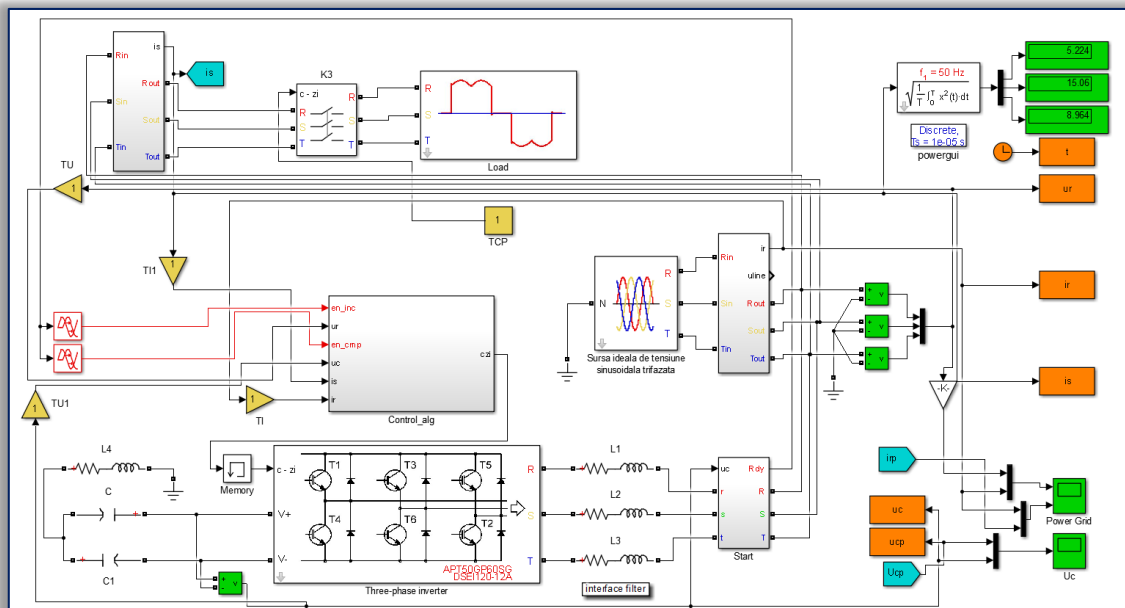


Figure 2. The active filtering system virtual model

It can be seen that the active power filter has the following specifications:

- ≡ Power grid:  $U_N = 400$  V
- ≡ First order interface filter –  $L = 3.7$  mH;
- ≡ Equivalent compensating capacitor  $550$   $\mu$ F;
- ≡ Power inverter transistors rated parameters:  $I_C = 100$  A,  $V_{CES} = 1200$  V

The initialization of the active power filter is done according to the typical steps [pemc]:

- ≡ The power section is connected to the grid by means of current limiting resistors (the capacitor is charged via the power inverter anti–parallel diodes);
- ≡ The resistors are short circuited when the compensating capacitor voltage reaches about 80% of the maximum voltage;
- ≡ The compensating capacitor is actively charged to the working voltage (the control loops are active), by absorbing from the power grid the necessary active current;
- ≡ The initial capacitor voltage is the voltage on the capacitor at the closed loop control system startup time.

Because the control algorithm was finally tested on an experimental system, at the plant site, the virtual nonlinear load was built to replicate the real current, absorbed by the industrial facility, sampled at a peak power consumption time.

The control algorithm is grouped in the *Control\_alg* block, in which, two sections can be observed, also grouped in subsystems (Figure 3):

- ≡ *Optimal parameters* – it contains the computations for the real time adjustment of the voltage controller parameters (imposed voltage,  $U_{cp}$ , proportionality constant,  $K_{pu}$ , and integration time constant,  $T_{iu}$ ), as a function of the load non–active power – Figure 4;

- It also contains the computation of the power grid phase voltage amplitude, necessary for the active power filter initialization process, as the imposed voltage ramp starts from this value (signal) and reaches the steady state value (which is the  $U_{cp}$  signal);
- It contains the computation of the load current active component amplitude;
- It is common to the both current control methods, although the load active current amplitude is used only by one of the two methods.

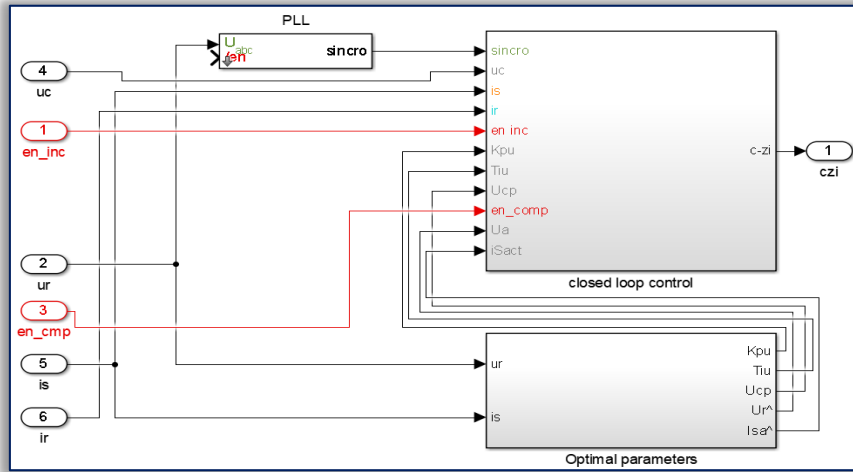


Figure 3. Detail of the control algorithm subsystem

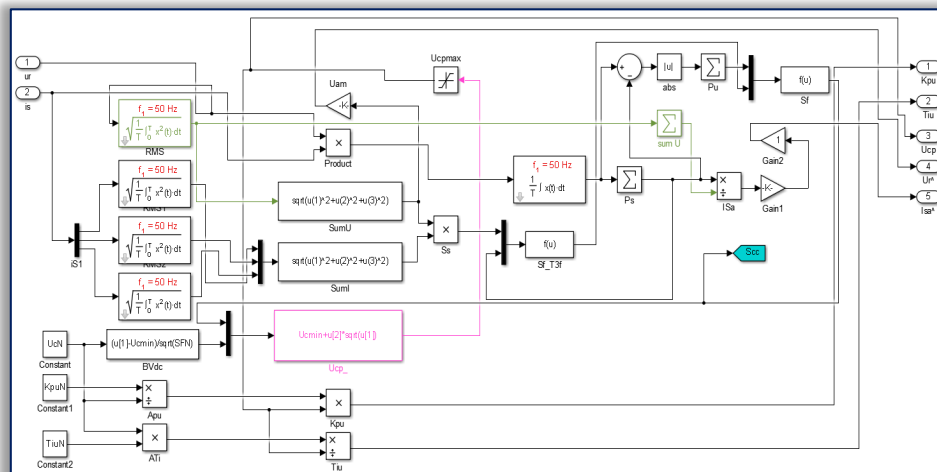


Figure 4. The Optimal parameters subsystem

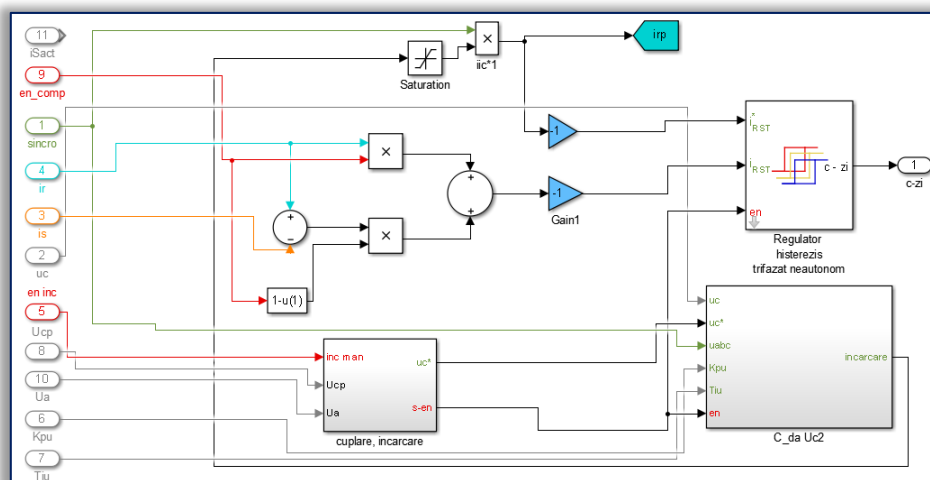


Figure 5. The closed loop control subsystem for the indirect current control method based on the voltage controller output



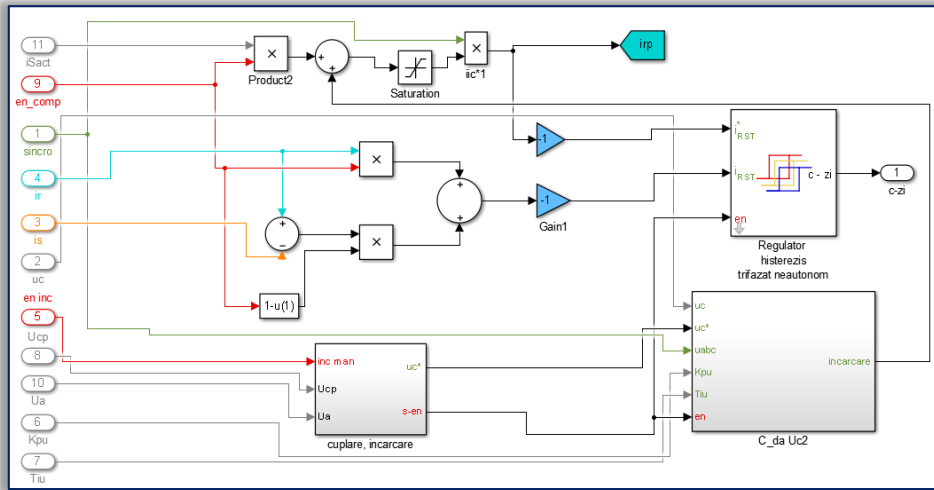


Figure 6. The closed loop control subsystem for the indirect current control method based on the load current active component

≡ *Closed loop control* – which contains the compensating capacitor voltage control loop, and the power grid absorbed current control loop; this subsystem is specific to the variant of the indirect current control, as seen in Figure 5 and Figure 6;

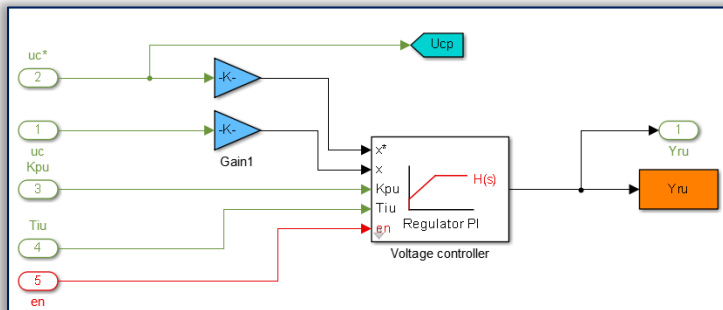
- o This is because the desired power grid current is obtained by multiplying the voltage controller output signal with the voltage template, received from the phase locked loop:
  - for the control method based on the voltage controller the power grid desired current amplitude is given only by the voltage controller – Figure 5;
  - for the control method based on the load current active component, the power grid desired current is given by the sum between the load current active component (which is also the desired compensated current) and the voltage controller output (which gives the active current drawn from the grid to charge the compensating capacitor and to cover the active power filter losses – Figure 6;

For the both indirect current control methods, the algorithm was adapted to allow the compensation validation from an external signal, although it cannot be done intrinsically. The voltage control loop and the current control loop are detailed in Figure 7, a and b.

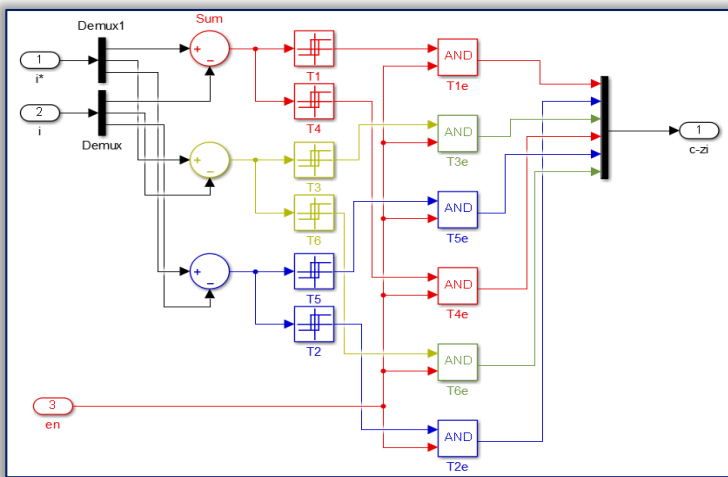
## 4. SIMULATION RESULTS

The simulation results had been obtained for the virtual models of the active filtering systems previously described, for a fixed simulation step of 1  $\mu$ s. Also, only the total compensation was considered as the current control based on the voltage regulator output cannot obtain the partial simulation (although, the other method could obtain this simulation goal).

The current absorbed by the nonlinear load from the power grid is illustrated in Figure 8. It can be seen that it is highly unbalanced, while at the same time, the current distortion is different on the three phases. The specific quantities are synthesized in Table 1.



a)



b)

Figure 7. The implementation of the closed loop control: a) the compensating capacitor voltage control loop, b) the desired grid current control loop

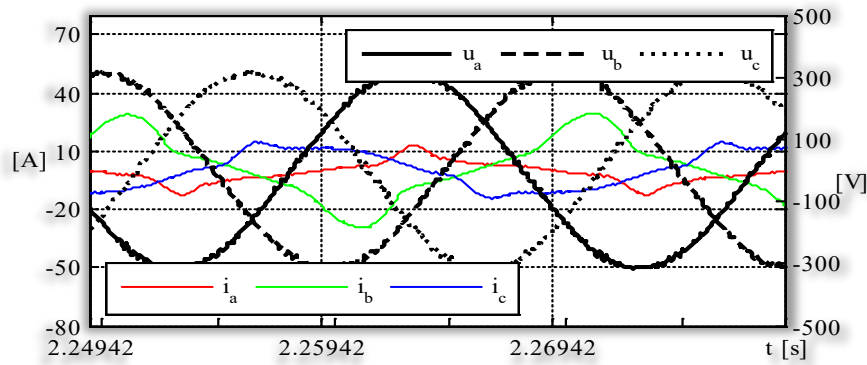


Figure 8. The virtual load current

Table 1. Nonlinear load power quality indicators

$I_a$ [A]	$I_b$ [A]	$I_c$ [A]	$THD_{i_a}$ [%]	$THD_{i_b}$ [%]	$THD_{i_c}$ [%]
5.22	15.06	8.96	34.47	26.72	13.13

After the compensation, the current absorbed from the power grid by the active filtering system is illustrated in Figure 9, for the two methods.

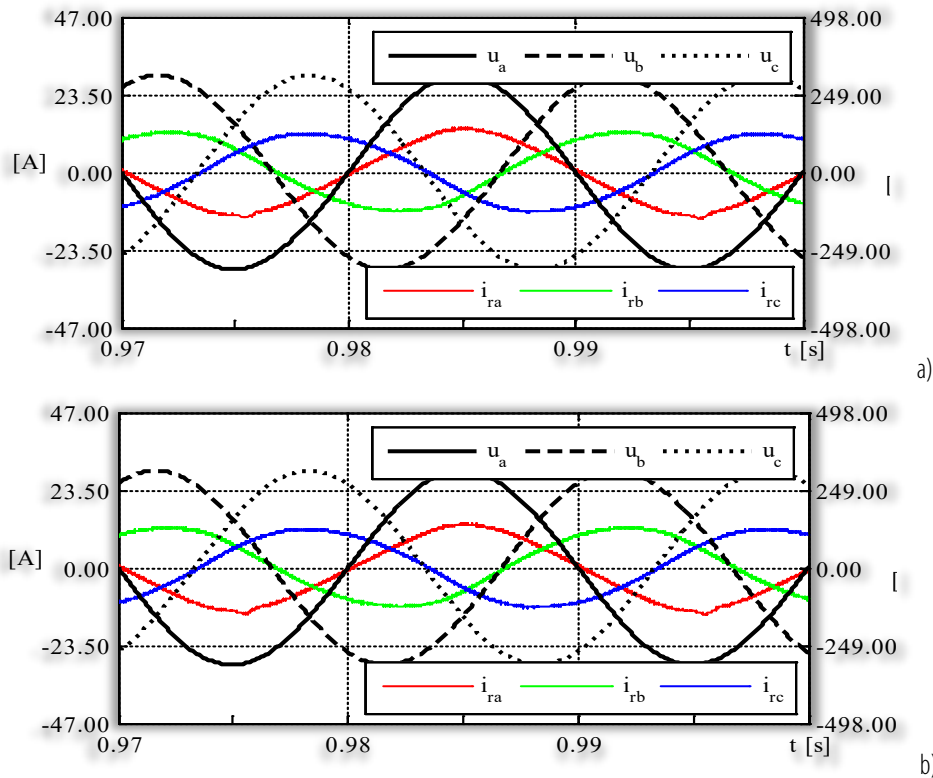


Figure 9. The power grid current for: a) the indirect current control method based on the voltage controller output, b) the indirect current control method based on the load current active component

It can be seen that qualitatively there is no noticeable difference between the power grid currents, for the investigated methods. The corresponding numeric results are synthetized in Table 2. It confirms that the two control methods lead to similar performance. Looking at the voltage controller output, it can be seen that when the desired grid current amplitude is obtained by the voltage controller, its output is significantly larger, than for the other case. Although, for the both cases, the voltage controller output ripple is the same, for different mean values. Because the grid desired current amplitude is given directly by the voltage controller for the first case, and by the sum between the voltage controller output and the load active component amplitude, the desired current amplitude ripple is the same for both cases, therefore the same imposed current distortion is produced.

It results that when the grid desired current amplitude is obtained by the voltage controller, it has a 1.94 A, for a 11.85 A mean value. When the grid current amplitude is obtained by summing the load current active component amplitude to the voltage controller output, the later has a 2.92 A mean value, and a 1.92 A ripple.

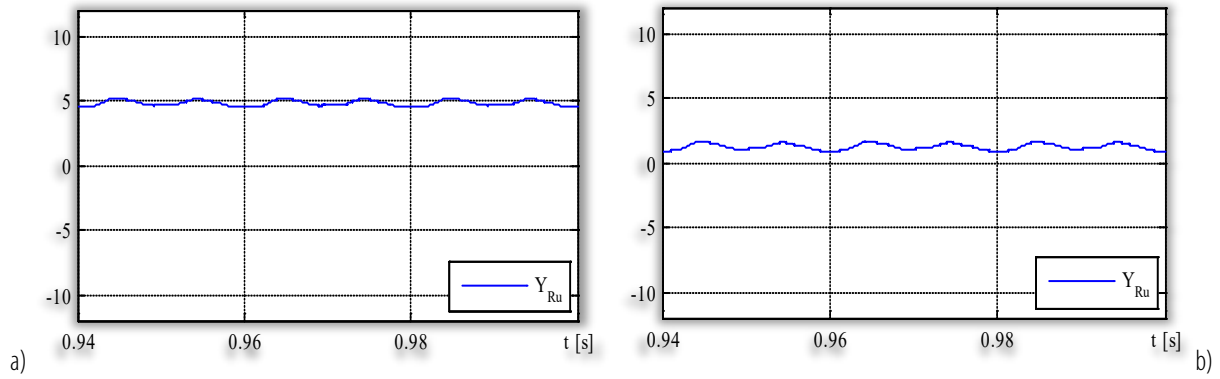


Figure 10. The voltage controller output for obtaining the desired grid current by: a) the voltage controller, b) the load active current

Table 2. Compensation results for desired current amplitude obtained from: a) the voltage controller, b) the load current active component

Current control	$I_a$ [V]	$I_b$ [A]	$I_c$ [A]	THD <sub>ia</sub> [%]	THD <sub>ib</sub> [%]	THD <sub>ic</sub> [%]	FE <sub>a</sub>	FE <sub>b</sub>	FE <sub>c</sub>
a	8.93	8.41	8.34	7.15	4.14	4.17	4.82	6.45	3.14
b	8.96	8.41	8.34	7.40	4.17	4.15	4.65	6.40	3.16

## 5. EXPERIMENTAL SETUP

The structure of the experimental active filtering system is illustrated in Figure 11. The experimental nonlinear load is a department of an industrial facility in Craiova, therefore the current to be compensated was dependent to the activities in the facility at the experiment time and couldn't been controlled.

The control of the active power filter is assured by a dSPACE ds1103 prototyping board, programed using the Matlab Simulink environment. This way, the control algorithm implemented on the virtual active filter was directly used to control the experimental active power filter. To obtained the real time control program of the latter, the subsystem containing the control algorithm (in Figure 3) was exported to another Simulink model where the section corresponding to the virtual power section of the active filtering system (SimPowerSystems blocks) was replaced to the Simulink blocks attached to the prototyping board hardware resources (i.e. the analog to digital converters and the digital I/O channels) – Figure 12 [9][12–14].

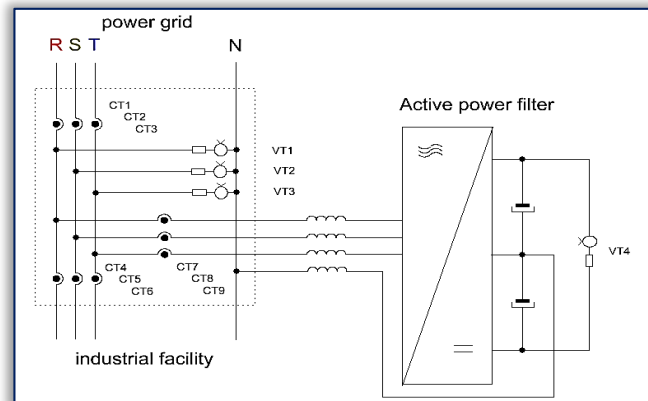


Figure 11. The experimental active filtering system diagram

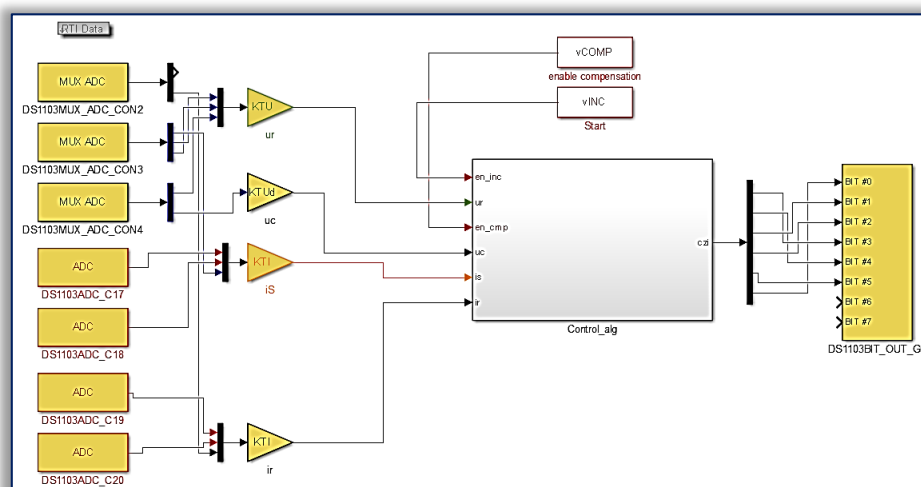


Figure 12. The experimental active power filter control algorithm

The system transducers (detailed in Figure 11) had been used to measure the system voltages and currents by the prototyping board. For this, the transducers output signals were assigned to a DS1103 board analog input, according to Table 3.



The real time control of the active filtering system is done by controlling the value of specific Simulink variables value in the control model (defined in the *Constant* blocks mask):

- ≡ Power section initialization – is done by the output of *Start* block (Figure 12) i.e. by the value of the Matlab variable *vINC*;
- ≡ Compensation validation – the compensation can be validated by the operator after the initialization process of the active filter is finished by the output signal of the *comp* block (the value of variable *vCOMP*):
  - this signal applies to the current controller all the active current to be absorbed from the power grid by the active filtering system, or just the active component necessary for the compensating capacitor charge and losses covering;
  - It also controls the feedback current components, in the same way.

The operation of the experimental active filtering system is controlled by means of a virtual control panel, built in Control Desk NG, the application software for the DS1103 – Figure 13. The virtual instruments of this panel are linked to the Simulink model signals and masked parameters. Thus, the control is assured by modifying the model parameters by means of the control panel, while the system monitoring and performance analysis is done by displaying the Simulink signals instantaneous value on the virtual oscilloscopes and panel meters. It worth mentioning that the quantities displayed by the panel meters are not really measured but computed in the control model by corresponding blocks (and their output signals being shown by the meter) [15–17].

Table 3. Prototyping board connection to the experimental active power filter power section

Transducer	ADC/IO Port	Signal	Connection
CT7	ADCH2	Filter output current (phase a)	P1A–34
CT8	ADCH4	Filter output current (phase b)	P1A–02
CT9	ADCH6	Filter output current (phase c)	P1A–19
VT1	ADCH10	Power grid voltage (phase a)	P1A–04
VT2	ADCH12	Power grid voltage (phase b)	P1A–21
VT3	ADCH14	Power grid voltage (phase c)	P1A–38
VT4	ADCH15	Compensating capacitor voltage	P1B–06
CT4	ADCH17	Load current (phase a)	P1B–23
CT5	ADCH18	Load current (phase b)	P1A–23
CT6	ADCH19	Load current (phase c)	P1B–04
CT1	ADCH19	Grid current (phase a)	P1B–40
CT2	ADCH20	Grid current (phase b)	P1A–40
CT3	ADCH8	Grid current (phase c)	P1A–36
–	IO3	T1 gate signal	P2A–02
–	IO4	T2 gate signal	P2B–19
–	IO1	T3 gate signal	P2A–18
–	IO2	T4 gate signal	P2B–02
–	IO0	T5 gate signal	P2B–18
–	IO10	T6 gate signal	P2B–04

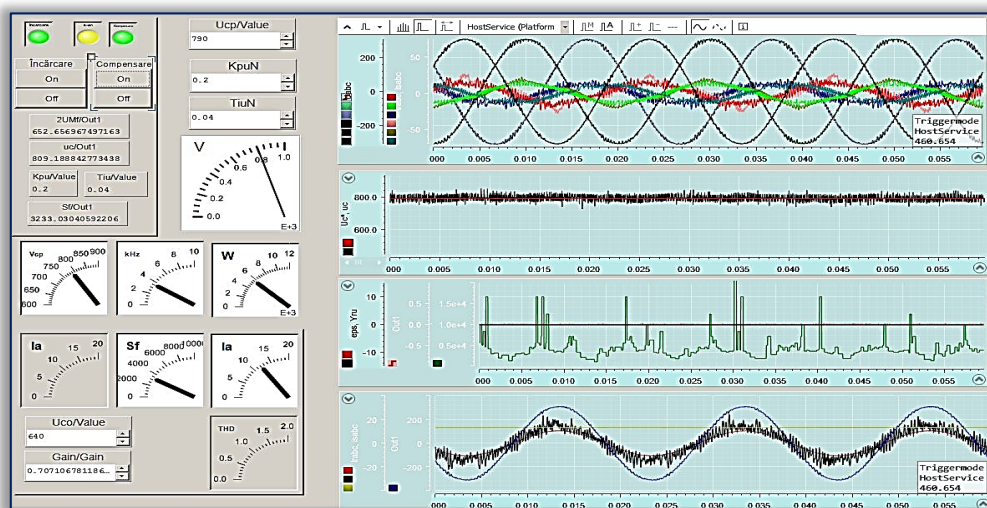


Figure 13. The active power filter real time control panel

## 6. EXPERIMENTAL RESULTS

The implemented control algorithm was experimentally tested at the plant site for a regular work day of the facility. Therefore, as stated above, the current to be compensated couldn't be controlled in any way. As a consequence, the experimental current to be compensated is not equivalent to the virtual one, for the two experiments.

The power quality indicators were measured using a Fluke 41b harmonic analyzer, and the instantaneous voltages and current were sampled with a Metrix OX7042 digital oscilloscope.

The first experiment corresponds to the indirect current control and the current to be compensated at the experiment time is illustrated in Figure 14. It can be seen that the current is highly unbalanced and the distortion



component of the current is dominant (compared to the reactive component). The power quality indicators, measured with the Fluke 41b harmonic analyzer are presented in Figure 15.

The power grid currents after the compensation are illustrated in Figure 16. It results that the compensated current is balanced and the reactive and distortion components are reduced. The filtering efficiency on the three phases is 5.1, 3.26 and 0.98, respectively.

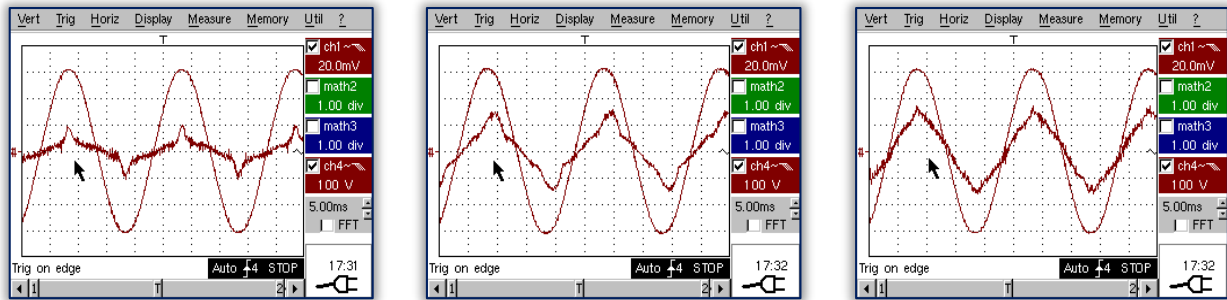


Figure 14. The power grid voltages and currents before compensation: phase (a), phase (b), phase (c)

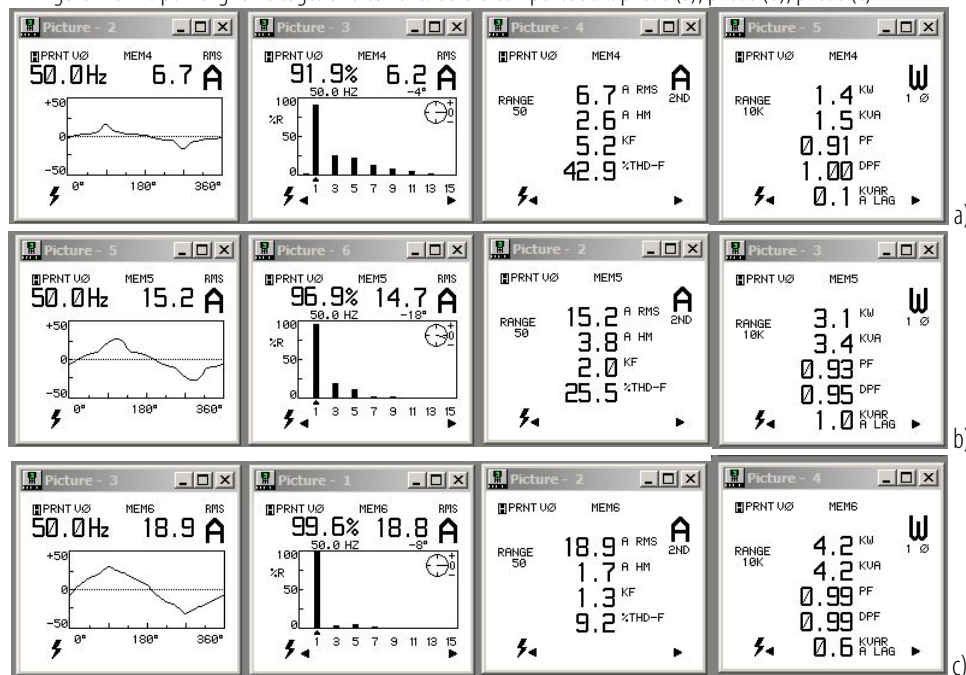


Figure 15. The power quality indicators before compensation: phase (a), phase (b), phase (c)

The experiments taken for the second case, which is the desired grid current amplitude obtained not only by the voltage controller, but by computing the load current active component were taken at a different moment of time, so the load current was slightly different at it results from Figure 18. The current waveforms are similar but the RMS values are smaller (with the corresponding effect on the total harmonic distortion factor).

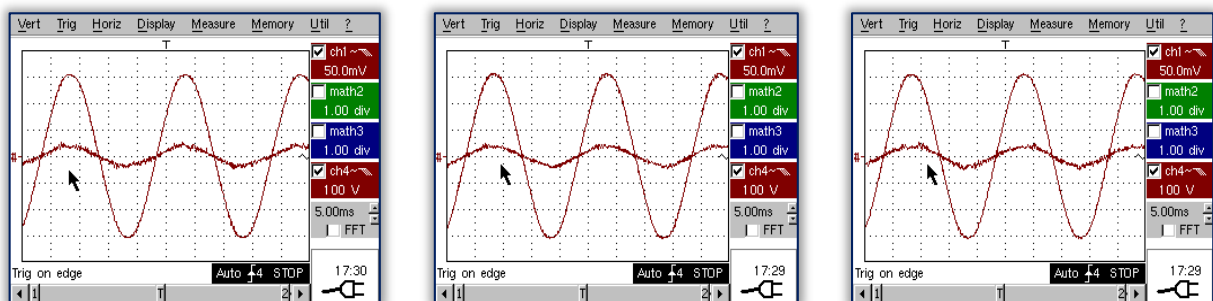


Figure 16. The power grid voltages and currents after compensation for the first control algorithm: phase (a), phase (b), phase (c)

The power quality indicators of these load currents are detailed in Figure 19. It can be seen that not only that the absorbed power is different from the previous experiment, but the power distribution on the three phases is different. The current distortion is also different.

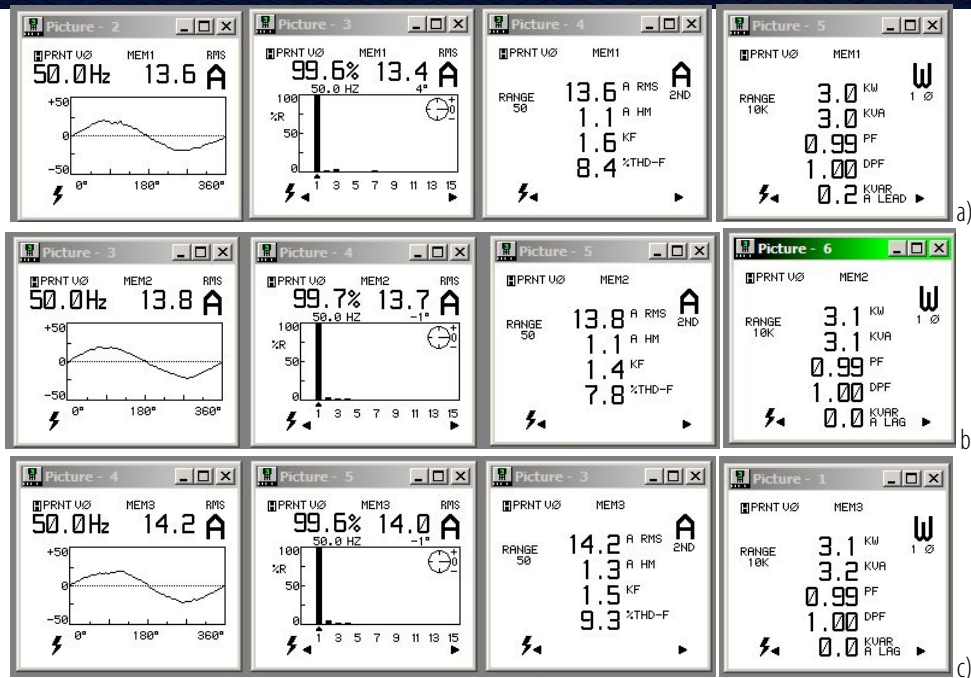


Figure 17. The power quality indicators after compensation for the first control algorithm: phase (a), phase (b), phase (c)

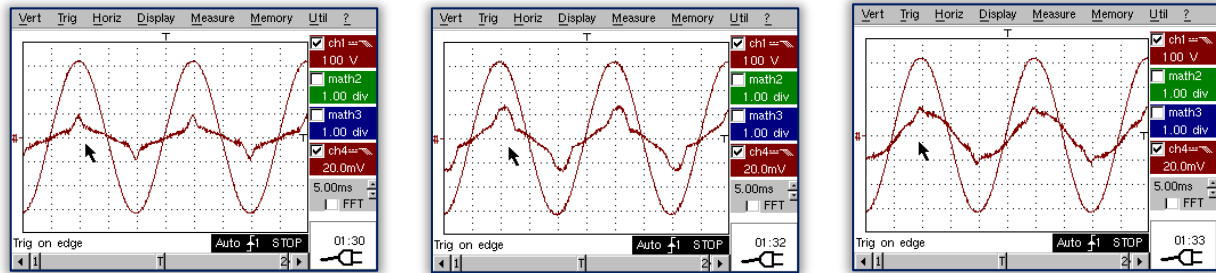


Figure 18. The power grid voltages and currents before compensation for the second control algorithm: phase (a), phase (b), phase (c)

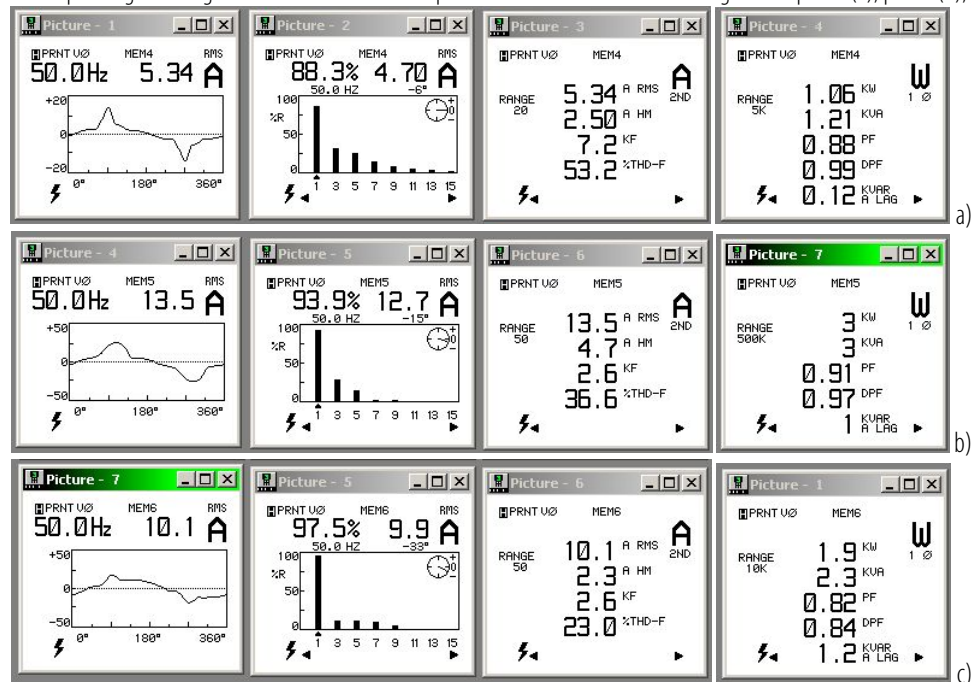


Figure 19. The power quality indicators before compensation for the second control algorithm: phase (a), phase (b), phase (c)

The current absorbed from the power grid after the compensation is illustrated in Figure 20. The current waveforms are better than for the previous case, qualitatively speaking. This is also proven quantitatively, as conformed by the power quality indicators in Figure 21. The filtering efficiency for this case, on the three phases is 9.33, 8.71, and 4.25, respectively. The significant difference between the results obtained by the two

implemented control algorithms is not given (only) by the difference between the load current at the experiments time, but by the desired power grid current amplitude obtained in the two ways. This is highlighted by the graphical representation of this two Simulink signals, sampled by the prototyping board at the experiment times, illustrated in Figure 22.

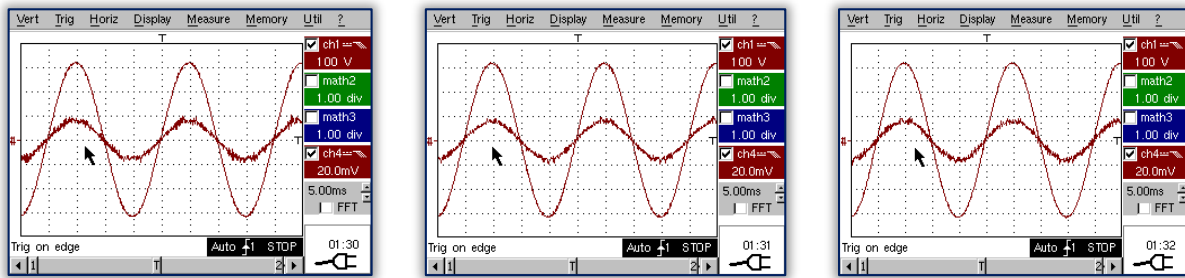


Figure 20. The power grid voltages and currents after compensation for the second control algorithm: phase (a), phase (b), phase (c)

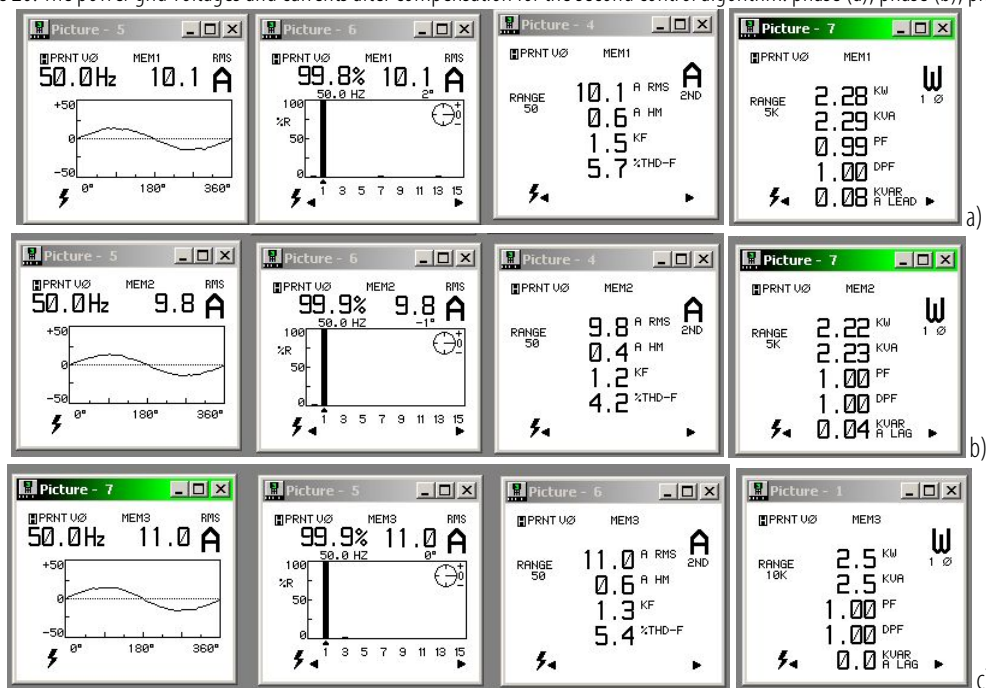


Figure 21. The power quality indicators after compensation for the second control algorithm: phase (a), phase (b), phase (c)

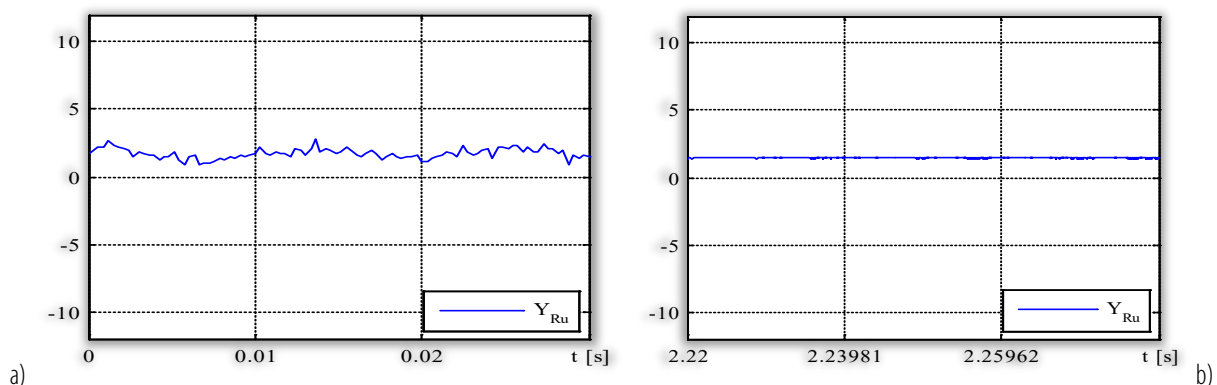


Figure 22. The desired grid current amplitude obtained: a) at the voltage controller output, b) computing the load current active current. The both signals in Figure 22 (showing the power grid current imposed amplitude) are normalized considering the rated current of the active filtering system.

In Figure 22–a, the voltage controller output has a significant high frequency ripple, given by the power inverter switching noise, but moreover, it has an important low frequency ripple, due to the voltage controller oscillations. In Figure 22–b, because the power grid current imposed amplitude is obtained by summing the voltage controller output with the load current computed amplitude of the active component (which is constant in steady state load operation), the voltage controller output is not only significantly lower, but significantly less noisy and less oscillating.



It must be mentioned, though, that the load absorbed power was a little lower at the second experiment time, observed in Figure 22 – the mean value of the current imposed amplitude in the right figure is a little lower than in the left figure.

## 7. CONCLUSIONS

- ≡ The control algorithm for the three phase four wire active filter was implemented in the Matlab Simulink environment for the two indirect current control methods.
- ≡ The correct implementation of the control algorithms was validated by simulation, giving similar results, but for a reasonable low simulation time step of 1  $\mu$ s.
- ≡ The implementation of the control methods was experimentally validated at the plant site. Considering the complexity of the experimental active filtering system, and also, the higher time step of 30  $\mu$ s, the results obtained by the indirect current control with the computation of the load current active component were significantly better than for the classical indirect current control.
- ≡ The system obtained performances could be improved by adjusting the system components – for the plant current at the experiment time, the optimal compensating capacitor voltage was higher than the voltage value limited by the system components.
- ≡ The active filtering system performances are highly dependent on the computing system time step therefore is important to have a high performance DSP in the active filter control section.

**Note:** This paper was presented at CNAE 2022 – XX<sup>th</sup> National Conference of Electric Drives, organized by University POLITEHNICA Timisoara, Faculty of Faculty of Electrotechnics and Electroenergetics (ROMANIA), in Timisoara, ROMANIA, in 12–13 May, 2022.

## References

- [1] Dovgun, V.; Temerbaev, S.; Chernyshov, M.; Novikov, V.; Boyarskaya, N.; Gracheva, E.: Distributed power quality conditioning system for three-phase four-wire low voltage networks, *Energies* 2020, 13, 4915.
- [2] Chebabhi, A.; Fellah, M.K.; Kessal, A.; Benkhoris M.F.: Comparative study of reference currents and DC bus voltage control for Three-Phase Four-Wire Four-Leg SAPF to compensate harmonics and reactive power with 3D SVM, *ISA Transactions* 2015, 57, pp. 360–372.
- [3] Barva, V.; Bhavsar, P.R.: Design and simulation of four-leg based three-phase four-wire shunt active power filter, In *Proceedings of 2018 International Conference on Communication information and Computing Technology (ICCICT)*, Mumbai, India, 2–3 Feb. 2018, pp. 1–6
- [4] Kaka, B.; Maji, A.: Performance evaluation of shunt active power filter (SAPF) connected to three phase four wire distribution networks, In *Proceedings of 2016 IEEE International Telecommunications Energy Conference (INTELEC)*, Austin, TX, USA, 23–27 Oct. 2016, pp. 1–9.
- [5] Bitoleanu, A.; Popescu, M.; Suru, V.: Theoretical and experimental evaluation of the indirect current control in active filtering and regeneration systems, In *Proceedings of the 2017 International Conference on Optimization of Electrical and Electronic Equipment*, Brasov, Romania, 25–27 May 2017.
- [6] Popescu, M.; Bitoleanu, A.; Suru, C.V.; Linca, M.; Subtirelu, G.E.: Adaptive control of DC voltage in three-phase three-wire shunt active power filters systems, *Energies* 2020, 13, 3147
- [7] Bitoleanu, A.; Popescu, M.; Suru, C.V.: *Filtre active de putere – Fundamente și aplicații*, Ed. Matrix Rom, București, 2021.
- [8] Popescu, M.; Bitoleanu, A.; Suru, V.: A DSP-based implementation of the p–q theory in active power filtering under nonideal voltage conditions, *IEEE Transactions on Industrial Informatics*, vol. 9, issue 2, May 2013, pp. 880–889.
- [9] Suru, V.; Popescu, M.; Pătrașcu, A.: Using dSPACE in the shunt static compensators control, *Annals of The University of Craiova*, no. 37, 2013, pp. 94–99.
- [10] Popescu, M.; Bitoleanu, A.; Suru, V.: Indirect current control in active DC railway traction substations, 2015 Intl Aegean Conference on Electrical Machines & Power Electronics (ACEMP), 2015 Intl Conference on Optimization of Electrical & Electronic Equipment (OPTIM) & 2015 Intl Symposium on Advanced Electromechanical Motion Systems (ELECTROMOTION), Electronic 2015
- [11] DS1103 Hardware Installation and Configuration for release 5.2, dSpace GmbH, 2006.
- [12] Real-Time Interface (RTI and RTI-MP) Implementation Guide for release 5.2, dSpace GmbH, 2006.
- [13] DS1103 PPC Controller Board, RTI Reference, Release 5.2 – December 2006.
- [14] Real-Time Interface (RTI and RTI-MP) Implementation Guide for release 5.2, dSpace GmbH, 2006.
- [15] Control Desk Experiment Guide for release 5.2, dSpace GmbH, 2006.
- [16] ControlDesk Next Generation Measurement and Recording Tutorial, For ControlDesk 5.3, Release 2014–B – November 2014
- [17] ControlDesk Next Generation Reference, For ControlDesk 5.3, Release 2014–B – November 2014.



ISSN 1584 – 2665 (printed version); ISSN 2601 – 2332 (online); ISSN-L 1584 – 2665

copyright © University POLITEHNICA Timisoara, Faculty of Engineering Hunedoara,  
5, Revolutiei, 331128, Hunedoara, ROMANIA  
<http://annals.fih.upt.ro>